A green approach to high-performance supercapacitor electrodes: chemical activation of hydrochar with potassium bicarbonate

Marta Sevilla,* Antonio B. Fuertes

Instituto Nacional del Carbón (CSIC), P.O. Box 73, Oviedo 33080, Spain

*Corresponding author: martasev@incar.csic.es

Abstract

Sustainable synthesis schemes for the production of porous carbons with appropriate textural properties for use as supercapacitor electrodes are in high demand. In this work a greener option to the widely used but corrosive KOH is proposed for the production of highly porous carbons. Hydrochar products are used as carbon precursors. It is demonstrated that a mild alkaline potassium salt such as potassium bicarbonate is very effective for generating porosity in hydrochar, leading to materials with large surface areas (> 2000 m^2 g^{-1}) and tunable pore size distribution. Furthermore, use of $KHCO_3$ instead of KOH gives rise to a significant 10% increase in the yield of activated carbon and the spherical morphology characteristic of hydrochar is retained, which translates into better packing properties and reduced ion diffusion distances. These features lead to a supercapacitor performance which can compete with, and even surpass, that of KOH activated hydrochar in a variety of electrolytes.

Keywords: activation, carbon material, porosity, supercapacitor, hydrochar

Introduction

Porous carbon materials are in high demand for a wide range of applications, such as catalysis,[1] energy storage (supercapacitors and Li-ion batteries),[2-4] energy production (electrocatalysts or electrocatalyst supports for fuel cells), [5-7] gas storage (H_2O, CH_4, CO_2) [2, 8] and the removal of contaminants (heavy metals, dyes, Hg, H_2S, SO_2, etc.).[9-11] Depending on the targeted application, specific chemical and/or structural properties are required. In the case of electrochemical capacitors or supercapacitors, porous carbons that combine an appropriate pore size distribution with large specific surface areas are needed. Indeed, several studies have shown that ion storage is more efficient in pores that match the size of the ions, whereas ion diffusion is facilitated by larger pores, which can also serve as electrolyte reservoirs. [12-15] In order to obtain materials with such controlled properties, a variety of synthesis methods have been developed, including nanocasting (soft- and hard-templating),[16-18] the selective etching of metals from metal carbides [19] or the direct carbonization of organic salts. [20, 21] More recently, a combination of different inorganic salts with soluble or liquid carbon precursors (*e.g.* glucose, ionic liquids) has led to the synthesis of micro-mesoporous carbons [22] or 3D hierarchical porous carbons. [23] However, these approaches fail to take advantage of the use of biomass or biomass wastes as carbon precursor, which are the most suitable carbon precursors for dealing with problems of economy, sustainability and availability. Therefore, in spite of the progress made so far, chemical activation of biomass and, especially KOH chemical activation, continues to be the preferred synthesis method for producing highly porous carbon materials (BET surface area > 2000 $m^2\ g^{-1}$) with a tunable porosity. [2] In this line of investigation, our

group was the first to show that activated carbons with advanced properties suitable for storing hydrogen could be produced by KOH chemical activation of hydrochar (*i.e.,* hydrothermally carbonized biomass).[24] Indeed, because of the heterogeneity and low carbon yield of biomass precursors, hydrochar is even a more appropriate carbon precursor. Since that work was published, we and other groups have synthesized high-performance carbons for CO_2 capture, [25-28] H_2 storage [27, 29] or supercapacitor electrodes [30-35] through that methodology. However, the industrial utilization of KOH activation is faced with economic and environmental challenges owing to its corrosiveness, which limits its use on a large scale. For this reason, more environmentally friendly alternatives for producing porous carbons than KOH activation must be explored. Accordingly, this work investigates the activation of glucose-derived hydrochar with a mild alkaline potassium salt, potassium bicarbonate. To date, this salt has only been used once to produce hierarchical porous carbons in conjunction with different kinds of biomass derivatives (*e.g.* starch, cellulose or glucose) and also biomass, *i.e.* bamboo. [36] Sodium bicarbonate has also been employed as activated agent with biochar (*i.e.,* pyrolyzed biomass) as carbon precursor, although this yielded a material with poor textural properties (*e.g.,* BET surface area of 550 m^2 g^{-1}). [37] This poor result is in agreement with previous reports that showed that sodium salts are less effective activating agents than potassium salts. [38, 39] In the present study it is demonstrated that potassium bicarbonate is very effective in generating porosity in hydrochar, resulting in materials with BET surface areas as high as 2300 m^2 g^{-1} and pore volumes of up to ~ 1.4 cm^3 g^{-1}. Furthermore, melamine-mediated $KHCO_3$ activation allows the synthesis of highly micro-mesoporous materials (S_{BET} > 3000 m^2 g^{-1}), as

efficiently as melamine-mediated KOH activation. Importantly, the use of potassium bicarbonate instead of potassium hydroxide leads to a significant increase in the yield of activated carbon. Furthermore, unlike KOH, it allows the spherical morphology of hydrochar to be retained, leading to better packing properties and reduced ion diffusion distances. This results in a supercapacitor performance which can compete with, and even surpass, that of KOH activated hydrochar.

Results and discussion

Chemical and structural properties of the activated carbons

For comparison purposes, glucose-derived hydrochar was activated with potassium hydroxide and potassium carbonate using the same (K/hydrochar) weight ratio as for potassium bicarbonate. Figure 1 shows SEM images of the hydrochar material produced from glucose at 180 ºC (Figure 1a) and its counterparts activated with $KHCO_3$ (Figure 1b), K_2CO_3 (Figure 1c) and KOH (Figure 1d). Whereas the spherical morphology is well preserved with $KHCO_3$ and K_2CO_3, KOH causes its complete destruction, generating irregular particles with conchoidal cavities, in agreement with the findings of previous works. [24-26, 32] Similar results were obtained for the hydrochar material synthesized at 240 ºC (Figure S1a). As revealed by the particle size distributions (insets in Figures 1a and 1b), the diameter of the spheres hardly changes from 380 ± 86 nm for the hydrochar synthesized at 180 ºC to 370 ± 76 nm in the case of the $KHCO_3$-activated hydrochar (similar results were obtained for the hydrochar synthesized at 240 ºC, as shown in Figure S1a). This is an encouraging achievement since uniform microspheres offer potential advantages such as good packing, a low

pressure drop and short diffusion distances. [40] On the other hand, as recently shown by Deng *et al.,* [36] when pure glucose is used as precursor instead of hydrochar, $KHCO_3$ causes its complete rearrangement giving rise to a 3D framework with large macropores (see Figure S1b), which suggests that a different activation mechanism is at work compared to that of hydrochar. As we stated in previous papers, [26] the complete rearrangement of the morphology of the particles that takes place when KOH is used as activating agent suggests that the hydrochar precursor is fragmented during the activation process, probably due to the melting of KOH at 360-380 ºC. However, K_2CO_3 does not melt until 890 ºC, which allows the preservation of the hydrochar particle's morphology with K_2CO_3 and $KHCO_3$ (the latter decomposing at ~150 ºC into K_2CO_3 according to the TG analysis in Figure S2a).

In order to verify the effectiveness of $KHCO_3$ as activating agent when using hydrochar as carbon precursor, N_2 physisorption analyses were performed. As can be seen in Figures 2a-b, all the isotherms are of type I -indicative of a microporous material- regardless of the activating agent or the hydrothermal carbonization temperature selected, as in the case of the carbonized hydrochar (HG180-850). However, the amount of nitrogen adsorbed depends substantially on the activating agent. In this case, porosity development follows the KOH > $KHCO_3$ ~ K_2CO_3 trend. The isotherm with the widest knee is the one corresponding to the material activated with KOH, *i.e.* HG180-KOH, suggesting a broader pore size distribution than that obtained with $KHCO_3$ and K_2CO_3. This is corroborated by the pore size distributions (PSDs) shown in Figures 2c-d. On the other hand, comparison of the isotherms corresponding to the activated carbons prepared from hydrochar materials

synthesized at 180 ºC (HG180-KB6) and 240 ºC (HG240-KB6) with the isotherm of the activated carbon produced from pure glucose (G-KB6) evidences that $KHCO_3$ generates more microporosity in the hydrochar material than in the case of pure glucose, where a broad PSD in the micro-meso-macropore range (see Figure 2c) is obtained, as reported by Deng *et al.* [36] Table 1 summarizes the textural properties of the porous carbons. As the isotherms showed, KOH is the activating agent that leads to the porous carbon with the largest BET surface area and pore volume, 2760 $m^2 g^{-1}$ and 1.3 $cm^3 g^{-1}$ respectively. However, $KHCO_3$ is also very effective for generating porosity in hydrochar, leading to materials with BET surface areas as high as 2230 $m^2 g^{-1}$ and pore volumes in the ~ 0.9 - 1.1 $cm^3 g^{-1}$ range. These values are similar to those obtained by K_2CO_3 activation (see Table 1), indicating that, in the case of hydrochar, the CO_2 generated by the decomposition of $KHCO_3$ does not play a significant role in pore development. This is coherent with the rigid structure of hydrochar and the fact that the CO_2 is generated at ~ 150 ºC. As can be seen in Table 1, when the $KHCO_3$/hydrochar weight ratio decreases from 6 (HG180-KB6) to 4 (HG180-KB4) or increases to 8 (HG180-KB8), carbons with slightly smaller surface areas and pore volumes are produced, ~ 2000 $m^2 g^{-1}$ and ~ 0.9 $cm^3 g^{-1}$ respectively. Especially worthy of note are the BET surface area values of the carbons produced from hydrochars HG180-KB6 and HG240-KB6, which are considerably higher than that of the carbon produced from glucose G-KB6 (1770 $m^2 g^{-1}$), owing to the enhanced micropore development in the hydrochar. This feature is of special interest for supercapacitor electrode applications since micropores are the most efficient types of pores for ion storage, too much meso/macroporosity leading to a low volumetric performance and electrolyte

flooding. [41] In this regard, measurement of the density of the electrodes (packing density) prepared with the different materials shows that the $KHCO_3$-activated carbons derived from hydrochar are the densest, whereas the $KHCO_3$-activated carbon derived from glucose is the least dense (Table 1).

In order to study the activation process in the presence of $KHCO_3$, a TG analysis was performed on the hydrochar impregnated with $KHCO_3$ and then compared to that of hydrochar. As can be seen in Figure S2b, carbonization of the hydrochar material takes place in the ~ 200 - 700 ºC range, resulting in a carbon yield of around 50 %. When $KHCO_3$ is present, there is a sharp weight loss at T < 200 ºC, which is attributed to the decomposition of $KHCO_3$ to K_2CO_3, in accordance with the TGA results in Figure S2a. The decomposition of the hydrochar takes place over a narrow range, *i.e.* 200 - 400 ºC. More importantly, at T > 700 ºC there is yet another sharp weight loss, which can be ascribed to the following redox reaction: [42, 43]

$$K_2CO_3 + 2\ C \rightarrow 2\ K + 3\ CO \qquad (1)$$

where the potassium carbonate is reduced by carbon to metallic potassium and the carbon is etched as CO, giving rise to the porosity detected by N_2 physisorption. In addition, potassium vapors may intercalate between the graphene layers, causing swelling and disruption of the carbon microstructure, thereby generating even more porosity. [20, 39] The occurrence of the above processes is supported by the detection of large white deposits corresponding to metallic potassium in the cool parts of the carbonization reactor. The fact that the reaction between K_2CO_3 and the hydrochar material takes places at T > 700 ºC is in agreement with the lower pore development obtained compared to KOH as the redox reaction between KOH and the hydrochar has already taken place

at that temperature. [38] On the other hand, the XRD pattern in Figure S3, which corresponds to sample HG180-KB6 before acid washing, reveals the presence of un-reacted K_2CO_3. As shown in Figure S2a, K_2CO_3 decomposes slowly at 850 ºC *via* the reaction:

$$K_2CO_3 \rightarrow K_2O + CO_2 \quad (2)$$

The CO_2 thus produced might partially gasify the carbon material (C + $CO_2 \rightarrow 2$ CO) and generate additional microporosity and/or enlarge existing pores. This suggests that increasing the residence time at 850 ºC could prove a successful strategy for increasing and/or modifying the porosity of the materials produced. Accordingly, we increased the residence time from 1 h to 3 and 5 h for the samples labeled HG180-KB6_3 and HG180-KB6_5. As can be seen in Figure 3a, the increase in residence time gradually enhances the amount of N_2 adsorbed at relative pressures higher than ~ 0.1, indicating the presence of larger pores. This is corroborated by the PSDs in Figure 3b, which show an increase in the amount of pores larger than ~ 2 nm. The textural data in Table 1 further confirm the increase in porosity with the extension of the residence time. Thus, the total pore volume experiences a 40 % increase when the residence time is extended from 1 to 5 h while the percentage of microporosity decreases from 84 % (1 h) to 63 % (5 h). Further proof of the gasification of carbon by the CO_2 produced from the slow decomposition of K_2CO_3 at 850 ºC is provided by the product yield, which decreases from 33 % (1 h) to 18 % (5 h).

In order to further enhance mesoporosity development in the $KHCO_3$-activated carbons, melamine was added to the $HKCO_3$/hydrochar mixture used in the activation process. We have recently shown that the KOH-chemical activation of biomass-derived hydrochar in the presence of melamine is an

effective approach for producing N-doped highly porous carbons (S_{BET} > 3000 m^2 g^{-1}) with a well-balanced micro-mesoporosity (V_{microp}/V_{mesop} ~ 1). [44, 45] Materials with these textural properties are very attractive for supercapacitors with bulky, viscous and low ionic mobility electrolytes such as room temperature ionic liquids (RTILs). [44] As can be seen from Figures 3c-3d, the addition of melamine with $KHCO_3$ as activating agent (HG180-KB6-M material) is just as effective for producing highly micro-mesoporous carbons as when KOH is used (HC180-KOH-M material). Thus, as shown by the PSD in Figure 3d, the HG180-KB6-M carbon exhibits a bimodal porosity similar to that of HG180-KOH-M, with maxima at ~ 0.9 and 2.3 nm, and a V_{microp}/V_{mesop} ratio equal to 0.84. The BET surface area of this material reaches a value of 3050 m^2 g^{-1} (Table 1), which is indicative of a high charge storage capacity. The SEM photos in Figures S4a-b show that the spherical morphology is also preserved in this case, although there is a certain agglomeration of microspheres. Also worth noting is that the packing density of the electrodes prepared with HG180-KB6-M is considerably higher than that of the HG180-KOH-M electrodes, *i.e.* 0.35 *vs.* 0.23 cm^3 g^{-1} respectively (Table 1). Moreover, bulk analysis of the material reveals a nitrogen content of ~ 4.2 wt.% (Table 1), with the homogeneous distribution of this heteroatom throughout all the particles as can be seen from the EDX mapping in Figure S4d. These results confirm the simultaneous N-doping and tuning of the PSD.

From an industrial point of view, an important feature to be taken into account is the product yield. This is especially the case when corrosive and harmful substances such as KOH are used. In Table 1 it can be seen that there is a substantial enhancement of the product yield for the samples activated with

$HKCO_3$ (33 % for HG180-KB6 and HG240-KB6) with respect to that activated with KOH (23 % for HG180-KOH). There is also a considerable economic advantage in that less activating agent is required to generate the same amount of product. In this regard, when hydrochar is used as carbon precursor instead of pure glucose, the yield experiences a *ca.* 4-fold increase (see Table 1), an improvement we also observed when using KOH. [26, 46] What is more, the HTC process can be optimized in order to obtain a large HTC yield (*i.e.* 34.4 %, HTC conditions: 240ºC - 1h, 1 M aqueous solution), so that the global product yield of the synthesis process (*i.e.* grams of activated carbon per 100 grams of raw material) exceeds that of pure glucose (11.3 % *vs.* 8.75 %). On the other hand, the yield achieved by K_2CO_3 chemical activation is similar to that of $KHCO_3$, which agrees with the fact that the same activation mechanisms are taking place in both cases. However, $KHCO_3$ has the advantage of being only mildly alkaline and less corrosive, so that it is safer to handle.

Electrochemical performance of the microporous carbons in aqueous electrolytes

Symmetric supercapacitors made up of two electrodes with similar carbon loadings of 8-11 mg cm^{-2} and electrode thicknesses of ~ 200-250 μm were used to analyze the electrochemical performance of the microporous carbons in 1 M H_2SO_4 and 1 M Li_2SO_4 electrolytes. A comparison of the galvanostatic charge/discharge voltage profiles (discharge current density of 0.1 A g^{-1}) in conventional H_2SO_4 electrolyte of the two materials produced by $KHCO_3$ activation (HG180-KB6 and HG240-KB6) and the material obtained by KOH activation (HG180-KOH) -in analogous activating conditions- is presented in Figure S5a. It can be seen that all the profiles are symmetric (coulombic

efficiency ~97-98 %) and quasi-rectangular, indicating a predominantly double-layer charge storage mechanism. The voltage profiles in Figure S5a also show that the HG180-KOH possesses a higher specific capacitance than HG180-KB6 and HG240-KB6, as revealed by its longer charge/discharge process. Indeed, as shown in Figure 4a, HG180-KOH exhibits an electrode specific capacitance of 270 F g^{-1} (106 F cm^{-3}) *vs.* 239 F g^{-1} (104 F cm^{-3}) in the case of HG180-KB6 and 246 F g^{-1} (105 F cm^{-3}) for HG240-KB6. However, the gravimetric capacitance of the materials activated with $KHCO_3$ is only 10-13 % smaller than that of the material activated with KOH. These values correlate well with the specific surface area of the materials, so that a surface area-normalized capacitance of 10-11 μF cm^{-2} is obtained in all cases. Figure 4b also shows that HG240-KB6 and HG180-KOH (54 and 51 % at 90 A g^{-1} respectively) have a similar rate capability, values which are both slightly superior to that of HG180-KB6 (46 % at 90 A g^{-1}). The slightly lower capacitance retention of HG180-KB6 may be explained by the somewhat narrower PSD and the fact that ion mobility is hindered to a greater extent in the mesopores between the particles than in the macroporous voids in HG180-KOH and HG240-KB6. [47, 48] On the other hand, the slightly better capacitance retention of HG240-KB6 compared to that of HG180-KOH is attributable to the shorter diffusion distances in HG240-KB6 owing to its smaller particle size (~ 0.6 μm). The high rate capability of all of these materials is evidenced by the voltage profiles in Figure S5b at the large discharge current density of 60 A g^{-1}. The profiles show only a small IR drop of 0.16-0.17 V. It is important to note that, when the electrode volume is taken into consideration (Figure 4a), the performance of the $KHCO_3$-activated carbons is even closer to that of the KOH-activated carbon, and even exceeds it at high

rates (> 10 A g^{-1}), which is a consequence of the better packing of the spherical particles preserved by $KHCO_3$ activation, compared to the irregular particles generated with KOH. Thus, optimization of the HTC conditions may lead to materials with better packing properties and a much improved volumetric performance.

The Ragone-like plot in Figure 4b further supports the competitive performance of the $KHCO_3$-activated carbons, especially from a volumetric point of view. Thus, the $KHCO_3$-activated carbons provide similar energy and power densities to the KOH-activated carbon both on a gravimetric and a volumetric basis. The KOH-activated carbon is able to deliver ~12-14 % more energy than the $KHCO_3$-activated carbons only at low rates and in gravimetric terms (*e.g.* 8.3 Wh kg^{-1} *vs.* 7.1-7.4 Wh kg^{-1} respectively at 0.12 kW kg^{-1}). The good electrochemical performance of these materials is further reinforced by their robustness, there being only a slight decrease of 1-2 % in capacitance after 5000 charge/discharge cycles at 5 A g^{-1} (see Figure S5c).

A comparative analysis of the electrochemical performance of the carbons activated with $KHCO_3$ (HG240-KB6) and KOH (HG180-KOH) was also carried out in a more user-friendly neutral aqueous electrolyte, *i.e.* Li_2SO_4. As can be seen from the symmetric voltage profiles in Figure 5a (coulombic efficiency ≥ 97 %) and the long-term cycling analysis results in Figure 5b, the supercapacitors are stable up to a voltage cell of 1.6 V in Li_2SO_4 compared to 1.0 V in H_2SO_4. However, the rate capability is lower in Li_2SO_4 than in H_2SO_4, as the $KHCO_3$-activated carbon is able to work up to 50 A g^{-1} (65 % capacitance retention) and the KOH-activated carbon only up to 15 A g^{-1} (63 % capacitance retention), as revealed by Figure 5c. It can be deduced from the Nyquist plots in

Figure S6 that the lower rate capability observed in Li_2SO_4 stems from its lower ionic conductivity compared to H_2SO_4, resulting in a higher equivalent series resistance (ESR) and a higher equivalent distributed resistance (EDR) and it is the latter parameter that mainly determines the total cell resistance. The Nyquist plots also show that the lower rate capability of the KOH-activated carbon is caused by a greater impedance to ion diffusion (*i.e.* EDR), a characteristic that we previously observed in other hydrochar-derived KOH microporous carbons. [45] We attribute the differences observed in ion diffusion kinetics to: i) shorter diffusion paths in the $KHCO_3$-activated carbon that is composed of spherical particles of diameter ~ 0.6 μm as opposed to irregular particles > 3 μm in width that make up the KOH-activated carbon (this factor is probably more important when a less conductive electrolyte is used), and ii) the more hydrophilic character of the $KHCO_3$-activated carbon. The higher wettability of the $KHCO_3$-activated carbon (which was at first visually observed) was confirmed by bulk elemental analysis and by temperature programmed desorption experiments (TPD). Thus, HG240-KB6 has a larger O content than HG180-KOH (Table 1), and the TPD experiments reveal the presence of a greater amount of carboxylic acids (in the 100 - 400 ºC range in the CO_2 desorption profile in Figure S7a) and of phenol groups (in the 600 - 700 ºC range in the CO desorption profile in Figure S7b) in HG240-KB6. Both of these types of oxygenated groups are known to improve wettability and reduce the resistance to ions diffusion inside micropores. [49, 50]

When the energy and power characteristics of these supercapacitors are drawn on a Ragone-like plot (see Figure 5d), the superior gravimetric and volumetric performance of the $KHCO_3$-activated carbon at high rates becomes

evident. These results demonstrate that high capacitance and high rate capability materials (*i.e.* materials with high energy-high power characteristics) can also be obtained with greener activating agents such as potassium bicarbonate. Comparison to the state-of-the-art in porous carbon materials further supports this statement (see Tables S1 and S2). Additionally, a comparison of the Ragone-like plots in Li_2SO_4 and H_2SO_4 electrolytes (Figures 5d and 4b respectively) shows an increase of *ca.* 50% in the amount of energy that can be stored by a supercapacitor assembled with $KHCO_3$-activated carbon, confirming that this electrolyte is an effective green alternative to the H_2SO_4 or KOH electrolytes that are currently in use.

Electrochemical performance of the bimodal micro-mesoporous carbons in ionic liquid electrolytes

A carbon with a bimodal pore structure made up of micropores ~ 0.9 nm wide and mesopores ~ 2.3 nm wide was synthesized by using as activating agent a mixture of $KHCO_3$ and melamine. Because this porous structure is ideal for bulky electrolytes such as RTILs, we examined the electrochemical performance of this material (HG180-KB6-M) in pure $EMImBF_4$ and a mixture of $EMImBF_4$ and acetonitrile (weight ratio 1:1). The rate capability of this material is compared with a material synthesized in similar conditions using a mixture of KOH and melamine (*i.e.* HG180-KOH-M) in Figure 6a. This reveals that both have a similarly high capacitance retention stemming from their micro-mesoporous structure, ~ 75 % at 30 A g^{-1} in pure $EMImBF_4$ and 73-78 % at 150 A g^{-1} in acetonitrile-diluted $EMImBF_4$. Figure 6a also shows that the dilution of the ionic liquid with acetonitrile boosts the rate capability, as a consequence of the much lower equivalent distributed resistance (ESR) of the cell (see voltages

profiles in Figure S8). Even though the gravimetric capacitance of the $KHCO_3$/melamine-activated carbon is slightly inferior to that of the KOH/melamine-activated carbon (by 10-15 %) owing to its smaller specific surface area (see Table 1), its volumetric capacitance surpasses that of the KOH/melamine-activated carbon by more than 25 % over the entire range of discharge rates (see Figure 6b) as a consequence of its greater packing density (see Table 1). These differences are also evident when the energy and power characteristics are represented on a Ragone-like plot (see Figure 6c). It is worth noting that the values of specific capacitance and rate capability of HG180-KB6-M are also competitive when compared to state-of-the-art carbon materials, including highly porous activated graphene or other activated carbons (see Table S3). In addition, Figure 6d shows that $KHCO_3$/melamine-activated carbon and KOH/melamine-activated carbon have similar charge/discharge cycling stabilities, with a capacitance retention which stabilizes at around 89-90 % after 4000 cycles in $EMImBF_4$ and at around 96-98 % after 1000 cycles in $EMImBF_4$/AN. This long-term stability matches that of other advanced carbon materials used as electrodes in IL-based supercapacitors.[51-54]

Conclusions

In summary, we have demonstrated that high performance supercapacitor electrodes can be produced by the chemical activation of hydrochar using a more environmentally friendly activating agent than KOH, *i.e.* potassium bicarbonate. This mild alkaline potassium salt is able to produce materials with BET surface areas as large as 2300 $m^2 g^{-1}$ and pore volumes of up to ~ 1.4 $cm^3 g^{-1}$. The pore size distribution is tuned either by adjusting the carbonization time or by adding melamine to the $KHCO_3$+hydrochar mixture. This last approach is

particularly effective for producing highly micro-mesoporous materials (S_{BET} ~ 3000 m^2 g^{-1}, V_{microp}/V_{mesop} = 0.84). The environmental benefits of potassium bicarbonate are accompanied by a 10% increase in the yield of the final product and the preservation of the hydrochar's spherical morphology, ensuring better packing properties and reduced ion diffusion distances. This results in a supercapacitor performance which can compete with, and even surpass, that of KOH activated hydrochar in a variety of electrolytes. On a gravimetric basis, the $KHCO_3$-activated carbons can store 3-3.6 Wh kg^{-1} *vs.* 3.4 Wh kg^{-1} for the KOH-activated carbon at 17 kW kg^{-1} in H_2SO_4, 10 Wh kg^{-1} *vs.* 7.9 Wh kg^{-1} at 7.5 kW kg^{-1} in Li_2SO_4, 16.1 kW kg^{-1} *vs.* 21.5 kW kg^{-1} at 19 kW kg^{-1} in $EMImBF_4$ and 19 Wh kg^{-1} *vs.* 25 kW kg^{-1} at 19 kW kg^{-1} in $EMImBF_4$/AN. On a volumetric basis, $KHCO_3$-activated carbons outperform KOH-activated carbons regardless of the electrolyte studied. More specifically, they can store 1.5-1.8 Wh L^{-1} *vs.* 1.5 Wh L^{-1} in the case of the KOH-activated carbon at 9 kW L^{-1} in H_2SO_4, 5.2 Wh L^{-1} *vs.* 3.9 Wh L^{-1} at 3 kW L^{-1} in Li_2SO_4, 8.5 kW L^{-1} *vs.* 5.3 kW L^{-1} at 4 kW L^{-1} in $EMImBF_4$ and 8.4 Wh L^{-1} *vs.* 5 kW L^{-1} at 14 kW L^{-1} in $EMImBF_4$/AN.

Experimental section

Synthesis of hydrochar materials

Hydrochar materials were prepared by the hydrothermal carbonization (HTC) of α-D-Glucose (96%, Aldrich). In brief, an aqueous solution of the raw material (0.5 M) was placed in a Teflon-lined stainless steel autoclave, heated up to 180 ºC and kept at this temperature for 5 h. Also, a 1 M aqueous solution of glucose was heat-treated at 240 ºC for 1 h. The resulting carbonaceous solids

(hydrochars) were recovered by filtration or centrifugation, washed with distilled water and dried at 120 ºC over a period of several hours.

Synthesis of porous carbon materials

The hydrochar materials were chemically activated using potassium bicarbonate (Sigma-Aldrich). In a first step, the hydrochar material was dispersed in a solution containing potassium bicarbonate ($KHCO_3$/hydrochar weight ratio = 4, 6 and 8). Afterwards, water was evaporated (under magnetic stirring) and the resulting mixture was heat-treated up to 850 ºC (heating rate: 5 ºC min^{-1}) under a nitrogen gas flow and held at this temperature for 1-5 h. The samples were then thoroughly washed several times with diluted HCl to remove any inorganic salts, then washed with distilled water until neutral pH was obtained and finally dried in an oven at 120 ºC for 3 h. The activated carbons produced by heat-treatment at 850ºC for 1 h were denoted as HG*x*-KB*y*, where *x* = HTC temperature and *y* = $KHCO_3$/hydrochar weight ratio (*i.e.* 4, 6 or 8). The materials produced by heat-treatment at 850 ºC for 3 and 5 h were labeled HG*x*-KB*y*_*z*, where *z* = 3 or 5 respectively. For comparison, raw glucose was activated using a $KHCO_3$/glucose weight ratio = 6 and labeled as G-KB6.

Bimodal micro-mesoporous carbons were produced by incorporating melamine into the activation process. Briefly, the hydrochar material was added to a dispersion containing potassium bicarbonate and melamine ($KHCO_3$/hydrochar weight ratio = 6 and melamine/hydrochar weight ratio = 2). After water evaporation (under magnetic stirring), the resulting mixture was heat-treated up to 800 ºC (heating rate: 5 ºC min^{-1}) under a nitrogen gas flow

and held at this temperature for 1 h. The activated carbon thus synthesized was denoted as HG180-KB6-M.

For comparison purposes, hydrochar materials produced by HTC of glucose (0.5 M) at 180 ºC (5 h) were also activated with potassium carbonate and potassium hydroxide. To keep the same proportion of K/hydrochar as in the case of $KHCO_3$ (*i.e.* K/hydrochar ~ 2.3), a K_2CO_3/hydrochar weight ratio = 4 and KOH/hydrochar weight ratio = 3.3 were used. These materials were denoted as HGx-KC and HGx-KOH, where *x* = HTC temperature. KOH activation was also carried out in the presence of melamine (KOH/hydrochar weight ratio = 3.3 and melamine/hydrochar weight ratio = 2). This carbon was labeled HG180-KOH-M.

Physical and chemical characterization

Scanning electron microscopy (SEM) images were recorded on a Quanta FEG650 (FEI) instrument. The particle size histograms were obtained by measuring ~ 300 particles in the SEM images. The nitrogen sorption isotherms of the carbon samples were measured at −196 °C using a Micromeritics ASAP 2020 sorptometer. The apparent surface area (S_{BET}) was calculated from the N_2 isotherms using the Brunauer-Emmett-Teller (BET) method. An appropriate relative pressure range was selected to ensure that a positive line intersect of multipoint BET fitting (C > 0) would be obtained and that the $V_{ads}(1 - p/p_o)$ would increase with p/p_o.[55, 56] The total pore volume (V_p) was determined from the amount of nitrogen adsorbed at a relative pressure (p/p_o) of 0.95. The micropore volume (V_m) was obtained by applying the Dubinin-Radushkevich equation.[57] The micropore size distributions were determined by applying the Quenched-Solid Density Functional Theory (QSDFT) method to the nitrogen

adsorption data and assuming a slit pore model. Elemental analysis (C, N and O) of the samples was carried out on a LECO CHN-932 microanalyzer.

Electrochemical characterization

The electrodes were composed of 85 wt% of active material, 10 wt% of polytetrafluoroethylene (PTFE) binder (Aldrich, 60 wt% suspension in water) and 5% of Super P (Timcal). The electrochemical measurements were performed in two-electrode Swagelok™ type cells in 1 M Li_2SO_4, 1 M H_2SO_4, $EMIMBF_4$ (1-ethyl-3-methylimidazolium tetrafluoroborate) and $EMIMBF_4$/acetonitrile (weight ratio 1:1) electrolyte solutions. The electrochemical capacitors were assembled using two carbon electrodes of comparable mass (carbon loading of 8-11 mg cm^{-2} in the case of the Li_2SO_4- and H_2SO_4-based supercapacitors and 5-6 mg cm^{-2} for the $EMIMBF_4$- and $EMIMBF_4$/AN-based supercapacitors) and thickness (200-250 μm), electrically isolated by a glassy fibrous separator. The electrochemical characterization was performed at room temperature using a computer-controlled potentiostat (Biologic VMP3 multichannel generator) and consisted of electrochemical impedance spectroscopy studies (EIS) and galvanostatic charge/discharge cycling tests.

Electrochemical impedance spectroscopy (EIS) measurements were performed at open circuit voltage (i.e. 0 V) within the frequency range of 1 mHz to 100 kHz and a 10 mV AC amplitude. Nyquist plots were recorded to characterize the impedance of the tested samples.

Galvanostatic charge/discharge cycling was performed between 0 and 1-1.6 V in aqueous electrolytes and in the 0-3 V range in ionic liquid electrolytes at increasing current densities from 0.1 to 150 A g^{-1}, based on the active mass

of one electrode. The specific gravimetric capacitance of one electrode determined from the galvanostatic cycles was calculated by means of the formula:

$$C_{sp} = \frac{4 \cdot I}{(dV/dt) \cdot m} \quad (2)$$

where I = current (A), dV/dt = the slope of the discharge curve (V s^{-1}) and m = mass (grams) of carbon material in the supercapacitor. As most supercapacitors are operated in the range of V_{max} to approximately ½ V_{max}, the upper half of the discharge curve was used to determine the slope of the discharge curve.[58]

To trace the Ragone plots, the specific energy (Wh kg^{-1}) and power (kW kg^{-1}) were calculated using the following formulae:

$$E = \frac{1}{2} C_{cell} \Delta V_d^{\,2} \quad (3)$$

$$P = \frac{E}{\Delta t_d} \quad (4)$$

where C_{cell} is the specific capacitance of the total cell (F g^{-1}), ΔV_d is the operation voltage ($V_{max} - IR_{drop}$) and Δ_{td} is the discharge time.

To calculate the specific volumetric capacitance, and volumetric energy and power densities, the packing density of the electrode was used. This density was determined from its thickness (measured with a micrometer caliper) and its area (0.785 cm^2).[59]

Acknowledgments

This research work was supported by the FICYT Regional Project (GRUPIN14-102) and Spanish MINECO (CTQ2015-63552-R) and Fondo Europeo de Desarrollo Regional (FEDER). The authors express their gratitude to Dr. M. D. Casal for the SEM pictures.

References

[1] F. Rodríguez-reinoso, *Carbon* **1998**, *36*, 159-175.
[2] M. Sevilla, R. Mokaya, *Energy Environ. Sci.* **2014**, *7*, 1250-1280.
[3] L. Wei, G. Yushin, *Nano Energy* **2012**, *1*, 552-565.
[4] N.-S. Choi, Z. Chen, S. A. Freunberger, X. Ji, Y.-K. Sun, K. Amine, G. Yushin, L. F. Nazar, J. Cho, P. G. Bruce, *Angew. Chem. Int. Ed.* **2012**, *51*, 9994-10024.
[5] M. Y. Song, H. Y. Park, D.-S. Yang, D. Bhattacharjya, J.-S. Yu, *ChemSusChem* **2014**, *7*, 1755-1763.
[6] F. Hasche, T.-P. Fellinger, M. Oezaslan, J. P. Paraknowitsch, M. Antonietti, P. Strasser, *Chemcatchem* **2012**, *4*, 479-483.
[7] W. Yang, T.-P. Fellinger, M. Antonietti, *J. Am. Chem. Soc.* **2011**, *133*, 206-209.
[8] A. Wahby, J. M. Ramos-Fernandez, M. Martinez-Escandell, A. Sepulveda-Escribano, J. Silvestre-Albero, F. Rodriguez-Reinoso, *ChemSusChem* **2010**, *3*, 974-981.
[9] S. F. Lo, S. Y. Wang, M. J. Tsai, L. D. Lin, *Chemical Engineering Research & Design* **2012**, *90*, 1397-1406.
[10] R. Yan, D. T. Liang, L. Tsen, J. H. Tay, *Environmental Science & Technology* **2002**, *36*, 4460-4466.
[11] J. H. Pavlish, E. A. Sondreal, M. D. Mann, E. S. Olson, K. C. Galbreath, D. L. Laudal, S. A. Benson, *Fuel Process. Technol.* **2003**, *82*, 89-165.
[12] J. Chmiola, C. Largeot, P.-L. Taberna, P. Simon, Y. Gogotsi, *Angew. Chem. Int. Ed.* **2008**, *47*, 3392-3395.
[13] J. Chmiola, G. Yushin, R. Dash, Y. Gogotsi, *J. Power Sources* **2006**, *158*, 765-772.
[14] J. Chmiola, G. Yushin, Y. Gogotsi, C. Portet, P. Simon, P. L. Taberna, *Science* **2006**, *313*, 1760-1763.
[15] C. Largeot, C. Portet, J. Chmiola, P.-L. Taberna, Y. Gogotsi, P. Simon, *J. Am. Chem. Soc.* **2008**, *130*, 2730-2731.
[16] H. Yang, D. Zhao, *J. Mater. Chem.* **2005**, *15*, 1217-1231.
[17] H. Nishihara, T. Kyotani, *Adv. Mater.* **2012**, *24*, 4473-4498.
[18] B. Sakintuna, Y. Yürüm, *Industrial & Engineering Chemistry Research* **2005**, *44*, 2893-2902.
[19] V. Presser, M. Heon, Y. Gogotsi, *Adv. Funct. Mater.* **2011**, *21*, 810-833.
[20] M. Sevilla, A. B. Fuertes, *J. Mater. Chem. A* **2013**, *1*, 13738-13741.
[21] B. Xu, D. Zheng, M. Jia, G. Cao, Y. Yang, *Electrochim. Acta* **2013**, *98*, 176-182.
[22] N. Fechler, T.-P. Fellinger, M. Antonietti, *Adv. Mater.* **2013**, *25*, 75-79.
[23] S. Zhu, J. Li, C. He, N. Zhao, E. Liu, C. Shi, M. Zhang, *J. Mater. Chem. A* **2015**, *3*, 22266-22273.
[24] M. Sevilla, A. B. Fuertes, R. Mokaya, *Energy Environ. Sci.* **2011**, *4*, 1400-1410.
[25] M. Sevilla, A. B. Fuertes, *Energy Environ. Sci.* **2011**, *4*, 1765-1771.
[26] M. Sevilla, C. Falco, M.-M. Titirici, A. B. Fuertes, *RSC Adv.* **2012**, *2*, 12792-12797.

[27] W. Sangchoom, R. Mokaya, *ACS Sustain Chem Eng* **2015**, *3*, 1658-1667.
[28] H. M. Coromina, D. A. Walsh, R. Mokaya, *J. Mater. Chem. A* **2016**, *4*, 280-289.
[29] J. Wang, I. Senkovska, S. Kaskel, Q. Liu, *Carbon* **2014**, *75*, 372-380.
[30] L. Wei, M. Sevilla, A. B. Fuertes, R. Mokaya, G. Yushin, *Adv. Energy Mater.* **2011**, *1*, 356-361.
[31] M. Sevilla, W. Gu, C. Falco, M. M. Titirici, A. B. Fuertes, G. Yushin, *J. Power Sources* **2014**, *267*, 26-32.
[32] C. Falco, J. Manuel Sieben, N. Brun, M. Sevilla, T. van der Mauelen, E. Morallon, D. Cazorla-Amoros, M.-M. Titirici, *ChemSusChem* **2013**, *6*, 374-382.
[33] H. Wang, Z. Xu, A. Kohandehghan, Z. Li, K. Cui, X. Tan, T. J. Stephenson, C. K. King'ondu, C. M. B. Holt, B. C. Olsen, J. K. Tak, D. Harfield, A. O. Anyia, D. Mitlin, *ACS Nano* **2013**, *7*, 5131-5141.
[34] G. A. Ferrero, A. B. Fuertes, M. Sevilla, *Scientific Reports* **2015**, *5*, 16618.
[35] D. Wang, Y. Min, Y. Yu, *J. Solid State Electrochem.* **2015**, *19*, 577-584.
[36] J. Deng, T. Xiong, F. Xu, M. Li, C. Han, Y. Gong, H. Wang, Y. Wang, *Green Chemistry* **2015**, *17*, 4053-4060.
[37] H. Jin, X. Wang, Z. Gu, J. D. Hoefelmeyer, K. Muthukumarappan, J. Julson, *RSC Adv.* **2014**, *4*, 14136-14142.
[38] M. A. Lillo-Ródenas, D. Cazorla-Amorós, A. Linares-Solano, *Carbon* **2003**, *41*, 267-275.
[39] E. Raymundo-Piñero, P. Azaïs, T. Cacciaguerra, D. Cazorla-Amorós, A. Linares-Solano, F. Béguin, *Carbon* **2005**, *43*, 786-795.
[40] G. A. Ferrero, A. B. Fuertes, M. Sevilla, *Electrochim. Acta* **2015**, *168*, 320-329.
[41] Y. Gogotsi, P. Simon, *Science* **2011**, *334*, 917-918.
[42] D. W. McKee, *Fuel* **1983**, *62*, 170-175.
[43] J. i. Hayashi, T. Horikawa, I. Takeda, K. Muroyama, F. Nasir Ani, *Carbon* **2002**, *40*, 2381-2386.
[44] A. B. Fuertes, M. Sevilla, *Carbon* **2015**, *94*, 41-52.
[45] A. B. Fuertes, M. Sevilla, *ChemSusChem* **2015**, *8*, 1049-1057.
[46] M. Sevilla, L. Yu, C. O. Ania, M.-M. Titirici, *ChemElectroChem* **2014**, *1*, 2138-2145.
[47] W. Gu, G. Yushin, *Wiley Interdisciplinary Reviews: Energy and Environment* **2014**, *3*, 424-473.
[48] C. Portet, G. Yushin, Y. Gogotsi, *J. Electrochem. Soc.* **2008**, *155*, A531-A536.
[49] J. Shen, A. Liu, Y. Tu, G. Foo, C. Yeo, M. B. Chan-Park, R. Jiang, Y. Chen, *Energy Environ. Sci.* **2011**, *4*, 4220-4229.
[50] Y.-T. Kim, T. Mitani, *J. Power Sources* **2006**, *158*, 1517-1522.
[51] T. Kim, G. Jung, S. Yoo, K. S. Suh, R. S. Ruoff, *ACS Nano* **2013**, *7*, 6899-6905.
[52] Z. Xu, Z. Li, C. M. B. Holt, X. Tan, H. Wang, B. S. Amirkhiz, T. Stephenson, D. Mitlin, *J. Phys. Chem. Lett.* **2012**, *3*, 2928-2933.
[53] L. Zhang, F. Zhang, X. Yang, G. Long, Y. Wu, T. Zhang, K. Leng, Y. Huang, Y. Ma, A. Yu, Y. Chen, *Sci. Rep.* **2013**, *3*.
[54] H. Zhang, K. Wang, X. Zhang, H. Lin, X. Sun, C. Li, Y. Ma, *J. Mater. Chem. A* **2015**, *3*, 11277-11286.
[55] in ISO 9277:2010. Determination of the specific surface area of solids by gas adsorption - BET method. Second Edition of ISO 9277, ISO, Vol. (Ed.^Eds.: Editor), City, **2012**.
[56] F. Rouquerol, J. Rouquerol, K. Sing, Adsorption by powders and porous solids: principles, methodology and applications, Academic Press, San Diego **1999**.
[57] M. M. Dubinin, *Carbon* **1989**, *27*, 457-467.
[58] M. D. Stoller, R. S. Ruoff, *Energy Environ. Sci.* **2010**, *3*, 1294-1301.
[59] A. B. Fuertes, G. A. Ferrero, M. Sevilla, *Energy Storage Materials* ***2016****, DOI: 10.1016/j.ensm.2016.05.002.*

Table 1. Physicochemical properties of the porous carbons obtained by chemical activation of hydrochar.

Carbon	Yield (%)[a]	Textural properties			Chemical composition [wt %]				Electrode density ($cm^3 g^{-1}$)[d]
		S_{BET} [$m^2 g^{-1}$]	V_p [$cm^3 g^{-1}$][b]	V_{micro} [$cm^3 g^{-1}$][c]	H	C	O	N	
HG180-850	50 (8)	525	0.22		-	-	-	-	-
HG180-KB6	33 (8)	2210	0.97	0.81 (84)	0.51	92.2	7.30	-	0.51
HG240-KB6	33 (34.4)	2230	1.05	0.84 (80)	0.41	93.7	5.65	-	0.50
HG180-KOH	23 (8)	2760	1.30	0.95 (73)	0.38	94.8	4.64	-	0.46
HG180-KC	34 (8)	2150	1.01	0.78 (77)	-	-	-	-	-
HG240-KC	36 (34.4)	2012	0.88	0.75 (85)	-	-	-	-	-
HG180-KB4	39 (8)	1996	0.87	0.76 (87)	-	-	-	-	-
HG180-KB8	34 (8)	2000	0.89	0.75 (84)	-	-	-	-	-
HG180-KB6_3	29 (8)	2130	1.04	0.79 (76)	0.42	94.2	5.33	-	-
HG180-KB6_5	18 (8)	2305	1.36	0.86 (63)	-	-	-	-	-
HG180-KB6-M	19 (8)	3050	2.10	0.96 (46)	0.71	88.5	6.63	4.16	0.35
HG180-KOH-M	17 (8)	3400	2.40	1.09 (45)	1.30	92.5	4.80	1.40	0.23
G-KB6	8.75	1770	1.07	0.65 (61)	-	-	-	-	0.43

[a] The yield of the HTC process is indicated in parenthesis. [b] Total pore volume was determined at a P/P_o of ~ 0.95. [c] The percentage of pore volume that corresponds to the micropores is given in parentheses. [d] The electrodes were pressed to 4 MPa.

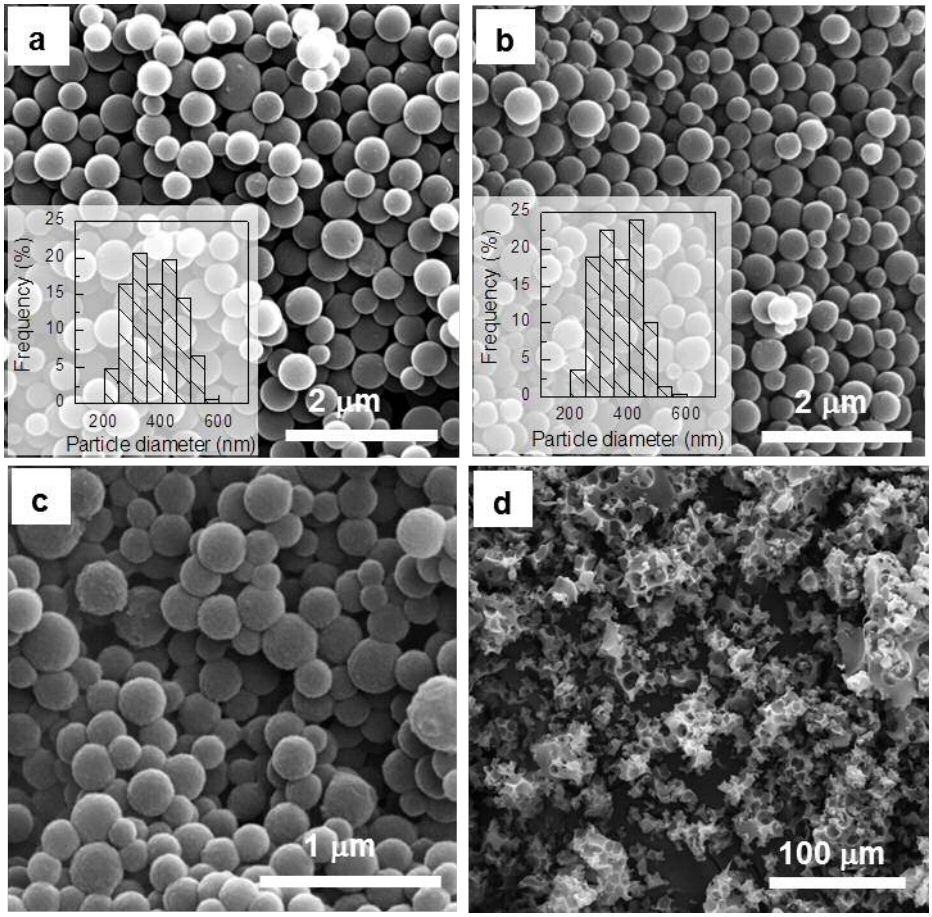

Figure 1. SEM images of (a) glucose-derived hydrochar synthesized at 180 ºC, and its counterparts activated with (b) $KHCO_3$, (c) K_2CO_3 and (d) KOH.

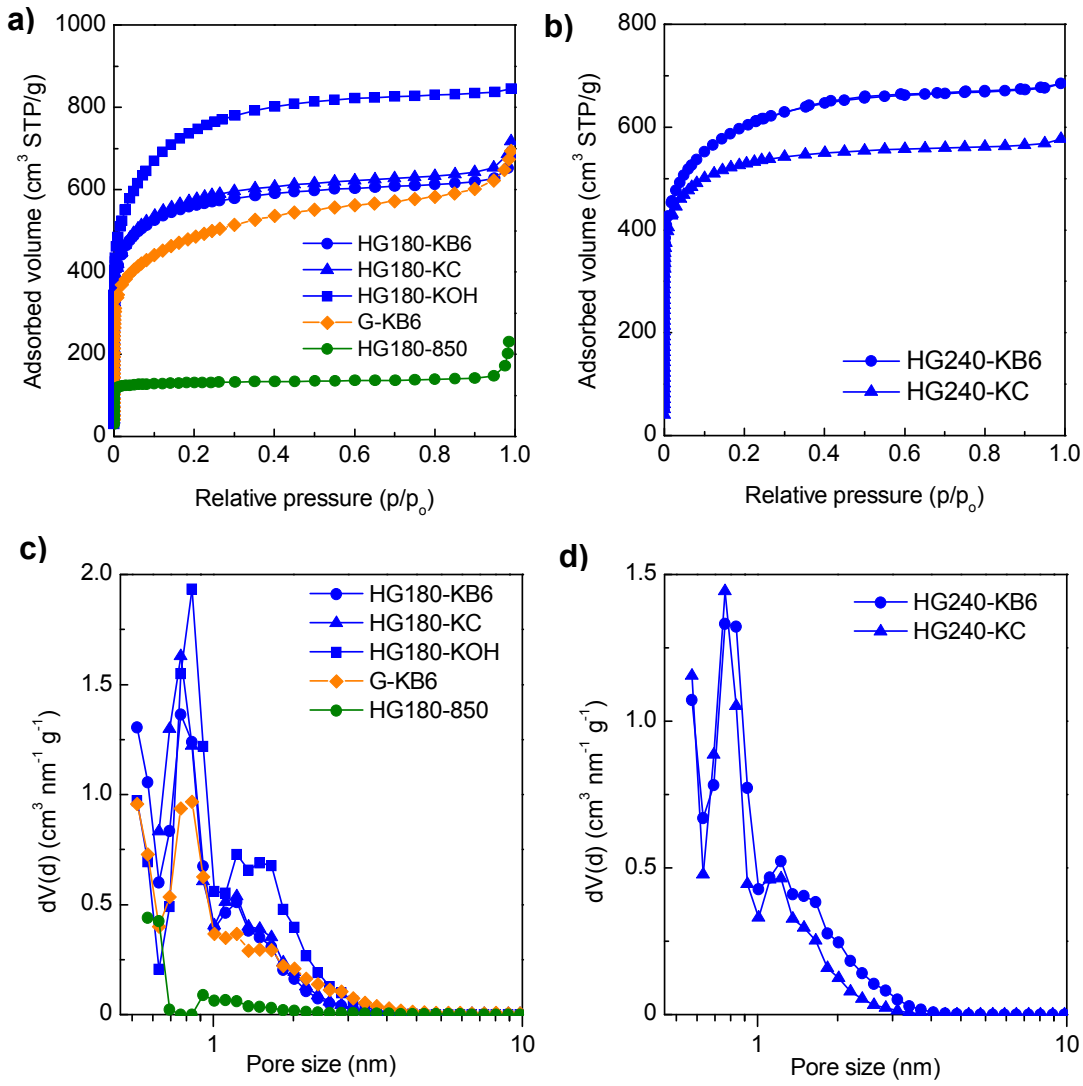

Figure 2. a, b) N_2 physisorption isotherms and c, d) QSDFT pore size distributions of the porous carbons synthesized from hydrochar produced at 180 ºC by using as activating agents $HKCO_3$ (HG180-KB6), K_2CO_3 (HG180-KC) and KOH (HG180-KOH), from hydrochar produced at 240 ºC by using as activating agents $HKCO_3$ (HG240-KB6) and K_2CO_3 (HG240-KC), and from pure glucose by using $HKCO_3$ (G-KB6).

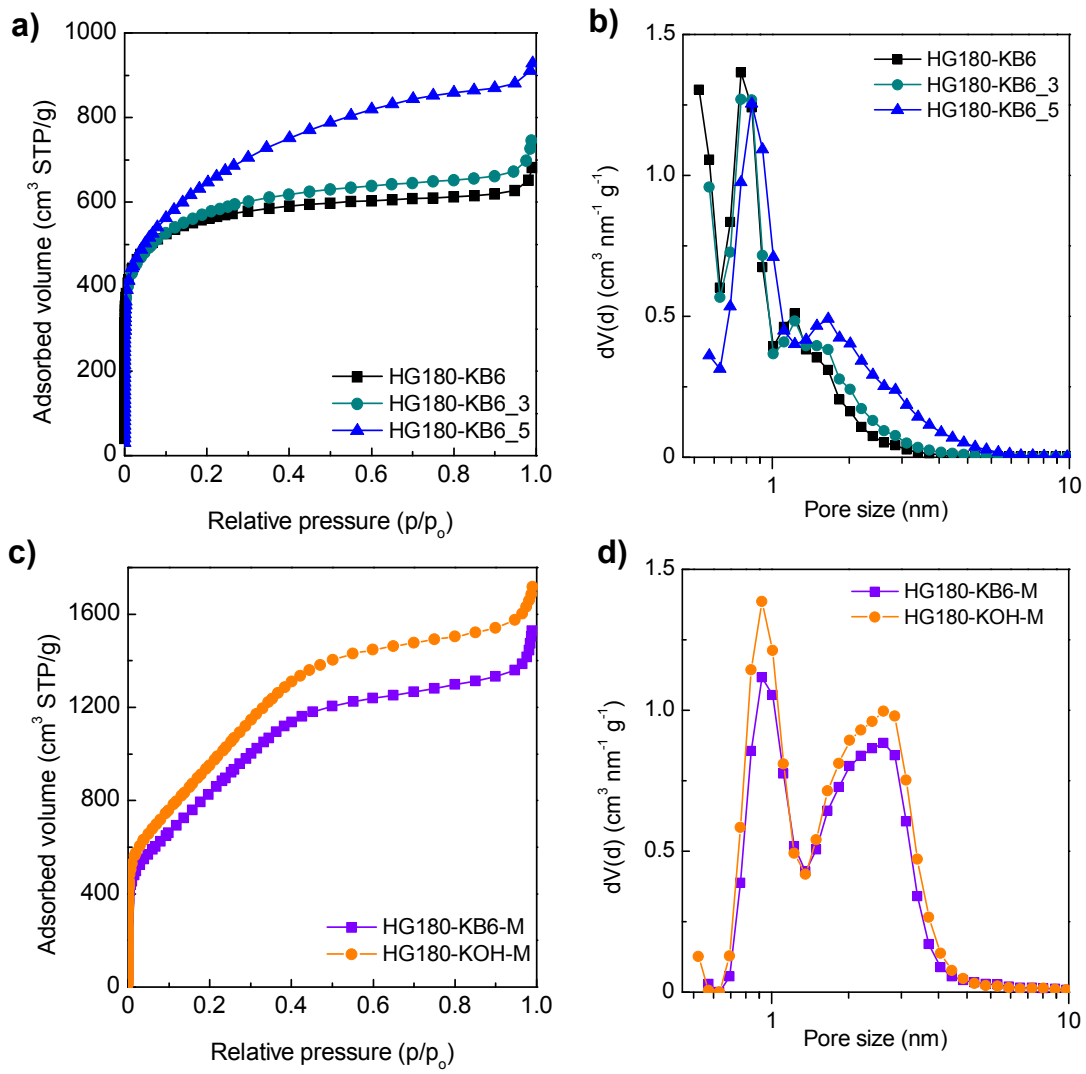

Figure 3. a) N_2 physisorption isotherms and b) QSDFT pore size distributions of the porous carbons produced from the hydrochar synthesized at 180 ºC and activated with $KHCO_3$ by increasing the residence time at 850ºC, c) N_2 physisorption isotherms and d) QSDFT PSD of the micro-mesoporous carbons produced in the presence of melamine (HG180-KB6-M and HG180-KOH-M).

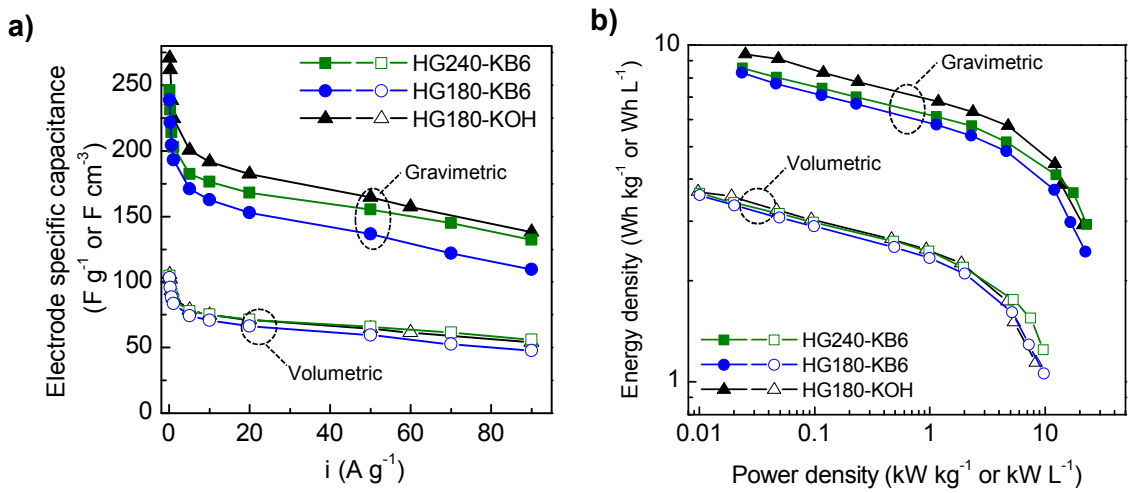

Figure 4. a) Evolution of the gravimetric and volumetric capacitance with the increase in discharge current density, and b) Ragone-like plot corresponding to the microporous carbons. Electrolyte: 1 M H_2SO_4.

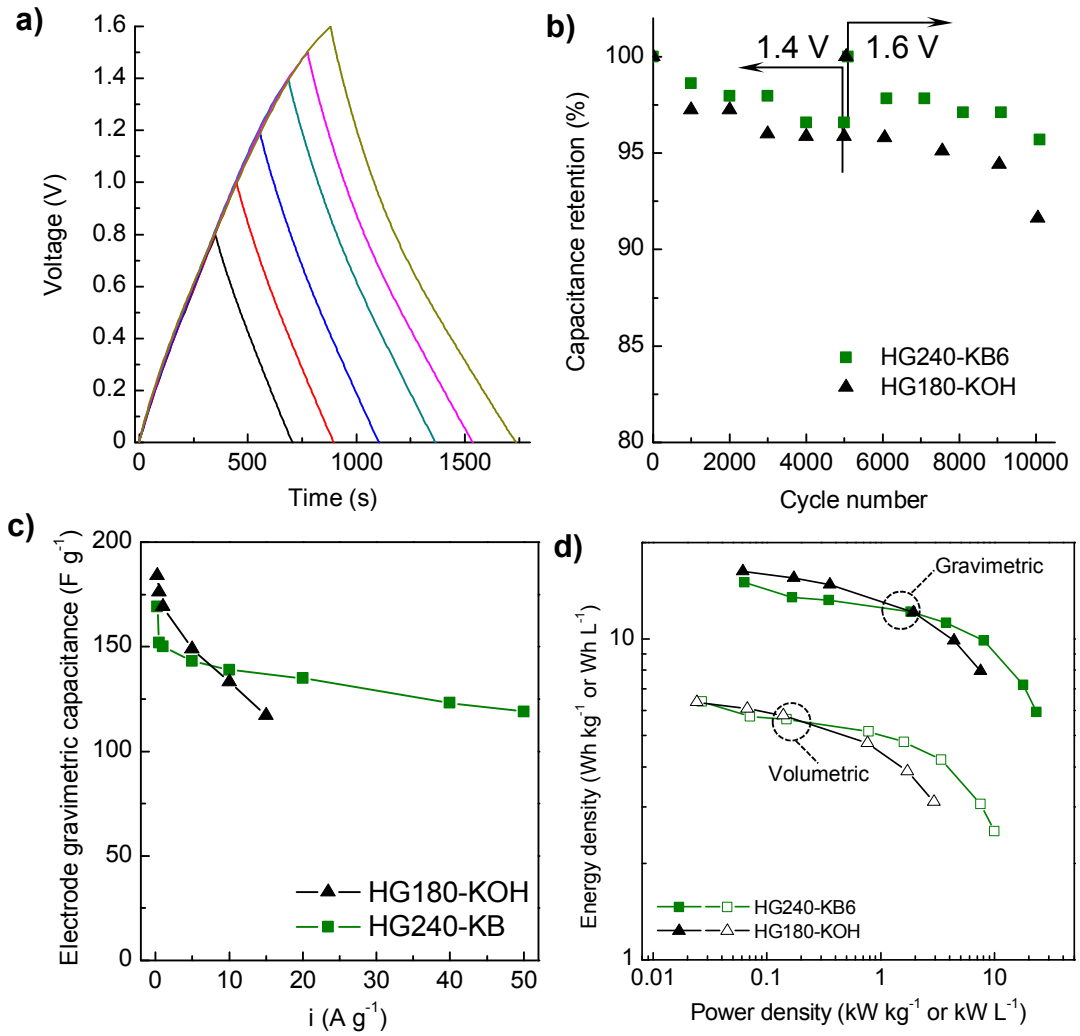

Figure 5. a) Constant current charge/discharge voltage profiles (0.2 A g^{-1}) at increasing cell voltage for HG240-KB6, b) capacitance retention evaluated by galvanostatic charge/discharge cycling at 5 A g^{-1} over 10000 cycles at two different cell voltages, c) evolution of the gravimetric capacitance with the increase in discharge current density and d) Ragone-like plot corresponding to the microporous carbons. Electrolyte: 1 M Li_2SO_4.

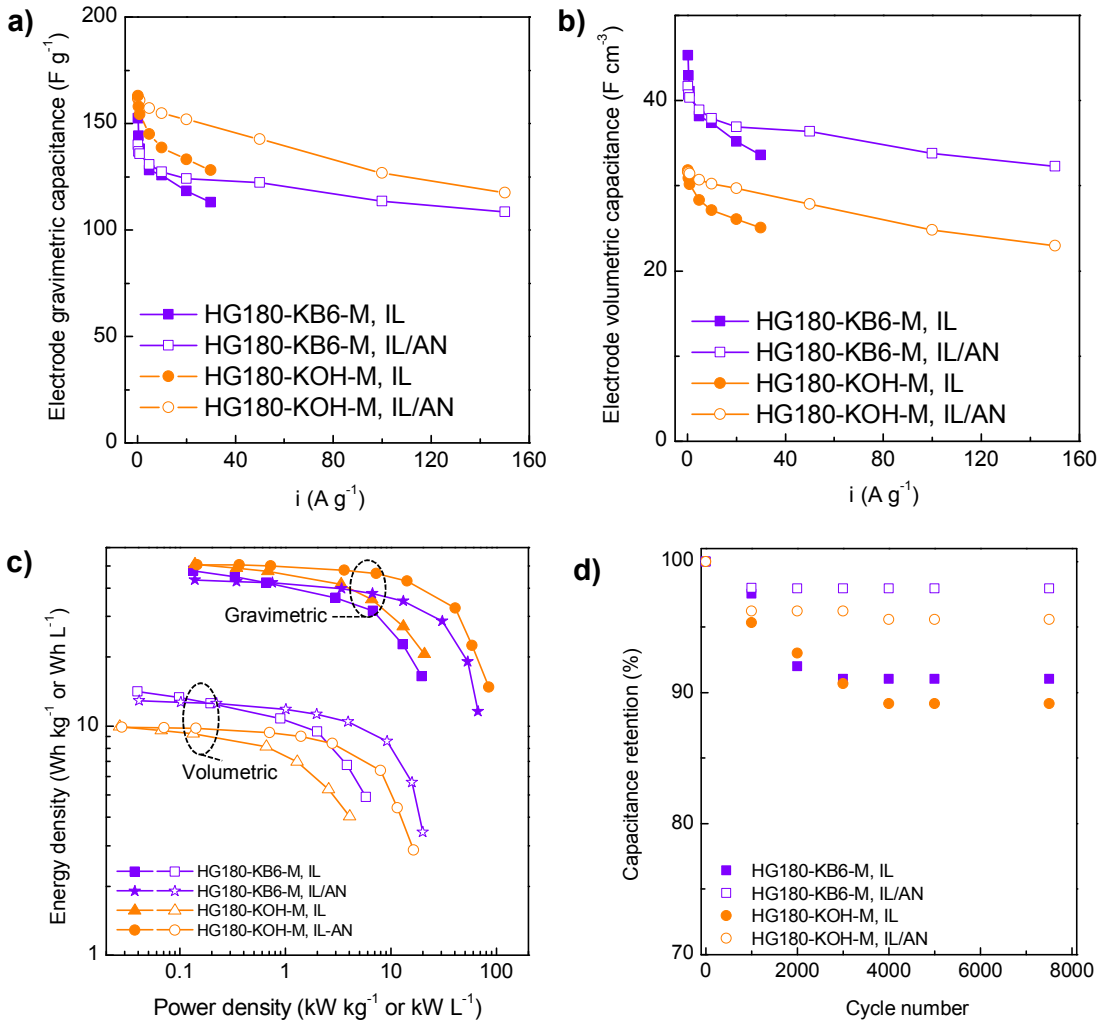

Figure 6. Impact of the increase in discharge current density on a) gravimetric capacitance and b) volumetric capacitance, c) Ragone-like plot and d) long-term cycling stability at 10 A g^{-1} and 3 V for the bimodal micro-mesoporous carbons. Electrolytes: room temperature $EMImBF_4$ and $EMImBF_4$/AN.

A green approach for the production of high-performance energy storage materials based on the activation of hydrochar with potassium bicarbonate is here successfully implemented.

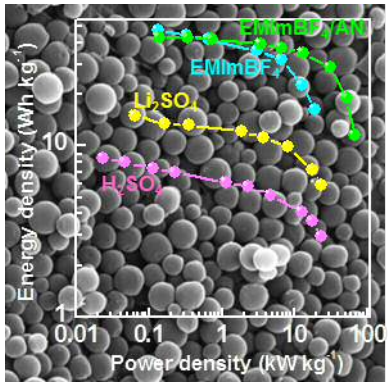

Marta Sevilla, Antonio B. Fuertes*

Page No. – Page No.

A green approach to high-performance supercapacitor electrodes: chemical activation of hydrochar with potassium bicarbonate